NJC

ARTICLE

Preparation of Ag Nanoparticles Using Hydrogen Peroxide as a Reducing Agent

Received 00th January 20xx,
Accepted 00th January 20xx

DOI: 10.1039/x0xx00000x

www.rsc.org/

Masamu Nishimoto,[a] Shigeaki Abe,[b] and Tetsu Yonezawa*[,a]

Herein, we report a method of Ag nanoparticle preparation using hydrogen peroxide as a reducing agent. Ag nanoparticles were synthesized using silver(I) nitrate as a silver precursor, aqueous NH_3 as a pH adjustor, and poly(vinyl pyrrolidone) (PVP) as a dispersant. The PVP concentration, reaction temperature, pH of the reaction solution, and silver precursor all had a great influence on the size of the Ag nanoparticles. These parameters affected the reduction speed of the Ag^+ ions and the aggregation of Ag nanoparticles. Ag nanoparticles of uniform shape were obtained under optimized conditions. In this work, we discuss a Ag nanoparticle growth mechanism based on La Mer's model, and aggregation control by PVP. This is a promising Ag nanoparticle preparation method with a low environment load.

Introduction

Ag nanoparticles (NPs) are widely used as conductive materials for electronics, such as solar cells and touch panels, due to the high electrical conductivity, pyroconductivity, and chemical stability of Ag. In addition, Ag NPs are known as a promising antimicrobial agent in the medical and dental field because Ag show antimicrobial activity and nontoxicity to human cells.[1-3] Chemical reduction,[4-9] plasma in liquid,[10-12] matrix sputtering,[13-16] and laser ablation[17] are known Ag NP preparation methods. Among these methods, chemical reduction is the most popular. Typically, reducing agents such as hydrazine and ascorbic acid are added to solutions containing metal ions and dispersants such as poly(vinyl pyrrolidone) (PVP) and poly(vinyl alcohol) (PVA). The metal ions are reduced by the reductant, and metal particles are generated. Chemical reduction is generally considered an easy and non-expensive method for generating metal NPs. Hydrazine, sodium borohydride, as well as ascorbic acid are famous reducing reagent to prepare Ag NPs and other metal NPs. However, hydrazine is toxic, borohydride changes to $B(OH)_3$ after reduction, and ascorbic acid is an organic compound which can be remained in the product dispersion, therefore, washing and water treatment processes are essential.

Recently, preparation methods for Au NPs and micron-sized Ag powders using hydrogen peroxide as a reducing agent have been reported.[18-24] In these cases, after NP formation, the byproducts of hydrogen peroxide are water and oxygen; therefore, impurities are not increased in the reaction solution. Moreover, residual hydrogen peroxide is more easily removed after the reaction than other reducing agents.

When Ag nanoparticles and H_2O_2 are mixed under neutral conditions, H_2O_2 acts as an oxidizing agent, and the surface of Ag nanoparticles are dissolved.[25,26] Ag^+ ions are reduced by H_2O_2 under neutral or acidic conditions, as shown in **Eq. 1** and **2**.[22,27] The standard Gibbs' free energies (ΔG^o) of these reactions are −9.7 and 33.2 kJ·mol^{-1}, respectively. Therefore, either the reaction is very slow or it does not occur. On the other hand, H_2O_2 acts as a reducing agent under alkaline conditions, and Ag^+ ions can be reduced to 0-valent Ag.[21-24] The reaction equation for the reduction of Ag^+ ions by H_2O_2 under alkaline conditions is shown in **Eq. 3**. The ΔG^o of this reaction was −50.2 kJ·mol^{-1}. Therefore, Ag^+ ions are reduced, and Ag metal atoms generated.

$$AgNO_3 + ½\ H_2O_2 \rightarrow Ag + ½\ O_2 + HNO_3 \quad (1)$$

$$[Ag(NH_3)_2]NO_3 + ½\ H_2O_2 \rightarrow Ag + ½\ O_2 + 2\ NH_3 + HNO_3 \quad (2)$$

$$[Ag(NH_3)_2]NO_3 + ½\ H_2O_2 + OH^- \rightarrow Ag + ½\ O_2 + H_2O + 2\ NH_3 + NO_3^- \quad (3)$$

It has been reported that micron-sized Ag powders, whose particle size is more than 1 μm, can be prepared using H_2O_2 as a reducing agent.[21-24] Chen *et al.* reported the preparation of fine Ag particles containing thick Ag plates (2 – 3 μm) and irregularly shaped particles with rough surfaces (1 – 2 μm).[21] In their method, 100 cm^3 of a 0.02 M silver nitrate solution was mixed with 1 cm^3 of 25% NH_3 in water. Then, 50 mm^3 of 30.62% w/v H_2O_2 was added to 5 cm^3 of a mixed silver ion solution. The reduction proceeded at 20 °C for 5 min. No

[a] Division of Materials Science and Engineering, Faculty of Engineering, Hokkaido University, Kita 13 Nishi 8, Kita-ku, Sapporo, Hokkaido 060-8628, Japan. E-mail: tetsu@eng.hokudai.ac.jp
[b] Department of Biomaterials and Bioengineering, Graduate School of Dental Medicine, Hokkaido University, Kita 13 Nishi 7, Kita-ku, Sapporo, Hokkaido 060-8586, Japan.

† Electronic Supplementary Information (ESI) available. See DOI: 10.1039/x0xx00000x

stabilizing agent was used. The Ag^+ ion concentration of this reaction solution was 0.02 M. Gatemala *et al.* reported a procedure for the preparation of fine Ag particles containing truncated cubes, icosahedra, and irregular particles (3 – 4 μm).[22] In this method, 1 cm^3 of a 1 M $AgNO_3$ solution was mixed with 1.7 cm^3 of a 5.3 M aqueous ammonia, and 10 cm^3 of a 5% w/v PVP solution. The pH of this solution was adjusted to ~ 10. Then, the total volume was adjusted to 97.7 cm^3 with deionized water. Finally, 2.3 cm^3 of 30% w/w H_2O_2 was added to the solution. The Ag^+ ion concentration of this reaction solution was 0.01 M. Gatemala et al. also reported a procedure for the preparation of fine Ag particles containing microplates, icosahedra, truncated cubes and quasi-spheres (2 – 100 μm).[23] In this method, a saturated solution of AgCl in 5.3 M NH_4OH was used as a Ag precursor solution. For example, a 90-mL of this Ag precursor solution was adjusted to pH 12.5 using 5 M NaOH and the total volume was adjusted to 182 mL by DI water. The solution was stirred for 5 min at room temperature (30 °C) with instantly adding H_2O_2 (30% w/w, 18 mL). Ag^+ ion concentration in this paper was varied from 0.1 to 0.58 M. When PVP was used as stabilizing agent, only microplates (10 – 20 μm) were obtained. Bai *et al.* also reported the formation of micron-sized Ag powders of an irregular shape (1 – 2 μm).[24] In their method, 20 cm^3 of a 0.15 M $AgNO_3$ solution was mixed with aqueous ammonia and a PVP solution (5 %/$AgNO_3$), then 10 cm^3 of 0.98 M H_2O_2 was added to the solution. The reduction proceeded at 30 °C for 10 min. The Ag^+ ion concentration of this reaction solution, and the volumes of aqueous ammonia and the PVP solution were not reported. When calculated using the concentrations of $AgNO_3$ and H_2O_2 solution, the Ag^+ ion concentration of this reaction solution was 0.10 M.

As mentioned above, micron-sized Ag powders with average particle sizes greater than 1 μm have been obtained using H_2O_2 as a reducing agent. However, to the best of our knowledge, no report on the preparation of Ag NPs by H_2O_2 reduction was published so far. Recently, we have proposed microwave induced plasma in liquid process with H_2O_2 as an additive for Ag NP preparation.[12] H_2O_2 had a positive influence on reduction of Ag^+ ions. In fact, it had also a positive influence on reduction of Au^{3+} ions[28] by plasma in liquid process.[29] Then, we became interested in the production of Ag NPs using only H_2O_2 as a reducing reagent especially for their applications in the field of bioscience and electronics. In this study, we have investigated the effects of PVP concentration, reaction temperature, pH of the reaction solution, H_2O_2 concentration, and silver precursors on the size of Ag NPs. Moreover, we tested the antimicrobial properties of Ag NPs against *Streptococcus mutans (S. mutans)* in order to evaluate the validity of the obtained Ag NPs.

Experimental Section

Materials

Silver(I) nitrate ($AgNO_3$, Kanto) and silver(I) oxide (Ag_2O, Wako) were used as silver precursors. Hydrogen peroxide (35%, Junsei) was used as a reducing agent. Aqueous ammonia ($NH_3 \cdot H_2O$) (28%, Junsei) was used as a pH control agent. Poly(vinyl pyrrolidone) (PVP, K-30, Junsei) was used as a dispersant. Potassium iodide (KI, Kanto) was used to quantify the amount of unreacted Ag^+ ions by producing AgI colloids which show an absorption peak at *ca.* 330 nm in UV-Vis spectra.[12,30] All chemicals were used as received. Deionized water (Organo/ELGA Purelabo system, >18.2 MΩ•cm) was used for the preparation of reaction solutions.

Preparation of Ag Nanoparticles

Silver(I) nitrate (4.08 mg) was added to 65 cm^3 of water, followed by the addition of 10 cm^3 of PVP (1.1 w/v%) aqueous solution, after which the solution pH was adjusted using aqueous ammonia (2.8%). This reaction solution was then heated up to the temperature indicated in **Table 1** under stirring at 500 rpm, followed by the addition of 5 cm^3 of hydrogen peroxide (0.15%). The reaction solution was kept stirred for 60 min at the prescribed temperature. Under the standard conditions, the concentration of Ag^+ ions, the molar ratios of PVP to Ag (PVP/Ag), and H_2O_2/Ag were 0.3 mM, 40, and 10, respectively. The molar concentration of PVP was calculated on the assumption that the molar mass of PVP is equal to 1 unit of PVP. To investigate the effect of the reaction conditions, PVP/Ag molar ratio, reaction temperature, pH, and H_2O_2/Ag molar ratio were varied within the range of 0 – 100, 50 – 90 °C, 10 – 12, and 0.6 – 10 respectively. In addition, Ag_2O was used to investigate the effect of different silver precursors on the silver nanoparticles. The reaction conditions conducted in this research are summarized in **Table 1**.

Table 1 Reaction conditions for the preparation of Ag nanoparticles.

Sample	PVP/Ag (mol/mol)	Reaction temp. / °C	pH	H_2O_2/Ag (mol/mol)	Ag precursor
1	0	80	10	10	$AgNO_3$
2	40	80	10	10	$AgNO_3$
3	100	80	10	10	$AgNO_3$
4	40	50	10	10	$AgNO_3$
5	40	90	10	10	$AgNO_3$
6	40	80	11	10	$AgNO_3$
7	40	80	12	10	$AgNO_3$
8	40	80	10	0.6	$AgNO_3$
9	40	80	10	1	$AgNO_3$
10	40	80	10	10	Ag_2O

Characterization

Transmission electron microscopy (TEM, JEOL JEM 2000-ES, at 200 kV) observation was used to analyse the size and morphology of the obtained Ag nanoparticles. For the preparation of TEM samples, the nanoparticle dispersion was dropped on collodion film-coated copper TEM grids, and naturally dried. The sizes of more than 200 Ag nanoparticles were measured manually from TEM images. X-ray diffraction (XRD, Rigaku MiniFlex-II, Cu Kα radiation, scanning rate of 10° min^{-1}) was used to analyze the composition. For the

preparation of XRD samples, the nanoparticle dispersion was filtered using a membrane filter (pore size = 0.2 μm), washed with water, and dried under ambient condition. The grain size of the obtained Ag NPs was calculated using Sherrer's equation which was applied to the largest peak (Ag(111)) at 38.2°.

The concentration of Ag^+ ions ($[Ag^+]$) after the reaction was determined in order to understand the reaction rate. The calibration curve for the $[Ag^+]$ concentration was prepared by using various concentrations of aqueous $AgNO_3$. Aqueous $AgNO_3$ (0.3 mM, PVP/Ag = 40) was diluted to prepare samples with various $[Ag^+]$ concentrations for this curve. KI (2.0 mg, 0.012 mmol) was added to 3 cm^3 of each sample solution with designated $[Ag^+]$ concentrations. UV-Vis spectra were collected immediately after the addition of KI using a UV-Vis spectrophotometer (Shimadzu, UV-1800) and a quartz cell with an optical path length of 1 cm. The calibration curve of the $[Ag^+]$ concentration was calculated using the area of the peak related to the coordination compound (PVP — $[Ag_mI_n]^{(n-m)-}$), which appears at approximately 330 nm.[12,30] Using this calibration curve, the amount of unreacted $[Ag^+]$ after the determination of the reaction.

Antibacterial test

The synthesized dispersions of Ag NPs were centrifuged, and then the precipitates were washed 5 times with deionized water. The dispersions of Ag NPs (around 3 g/L) were prepared by the addition of deionized water to the final precipitates. The Ag concentrations of these dispersions were analysed by an ICP Emission Spectrometer (Shimadzu, ICPE-9000).

S. mutans was cultivated in the brain heart infusion (BHI) broth (3.7 g BHI broth and 100 mL H_2O), and then incubated overnight at 37 °C in an incubator. The preparation procedure of the agar plate medium is as follows. BHI broth (3.7 g) was dissolved in H_2O (100 mL), and then 1.5% of agar and 5% of sucrose were added. This medium was sterilized at 120 °C for 20 min in an autoclave. After cooling, this medium was poured into a dish and cooled until the medium became solid.

The BHI broth containing *S. mutans* (100 μL) were coated on the agar plate medium, and then the dispersions of Ag NPs (5 μL) were spotted. The Ag concentrations of the dispersions were 0.001, 0.01, 0.1, and 1 g/L. The medium was incubated at 37 °C in an atmosphere of 5% CO_2 for 20 hours. The zone of inhibition was observed by eyes.

Results and discussion

Effect of PVP Concentration

PVP has been utilized as a dispersant to produce silver nanoparticles. PVP has a very low gold number and has been frequently used for the stabilization of metal nanoparticles.[31,32] Therefore, well-dispersed silver nanoparticles could be obtained under a low PVP concentration.[33] **Figure 1** shows TEM images and particle size distributions of Ag nanoparticles (NPs) obtained under various molar ratios of PVP to Ag. Without PVP (PVP/Ag = 0, Sample 1), the average particle size was 236.1 nm, and irregular particles were obtained. At PVP/Ag molar ratio was 40 (Sample 2), the average particle size was 89.7 nm, and spherical and a small amount of polygonal particles were obtained. Larger particles shows polygonal faceted structures in the TEM image. When PVP concentration was further increased (PVP/Ag = 100, Sample 3), the average particle size was 115.8 nm, and a mixture of larger spherical particles and small spherical nanoparticles around 20 nm were obtained. It has been reported that homogenous Ag nanoparticles or nanocubes were synthesized using PVP as a dispersant and ethylene glycol as a solvent and reducing agent.[34] The morphology of the Ag nanoparticles shown in **Figure 1** was not much more uniform than previous reports. We consider that the reducing rate will affect the morphology of Ag nanoparticles. In our experiments, the colors of the reaction solution were changed immediately after the addition of H_2O_2. The reduction of Ag^+ ions was completed soon. Therefore, PVP was not able to adsorb on the Ag cluster before the particle growth. As a result, the morphology of obtained Ag nanoparticles was spherical and heterogeneous. X-ray diffraction patterns of the obtained Ag NPs are shown in **Figure 2** and the inset grain sizes were calculated using Sherrer's equation which is applied to the largest peak at 38.2° (Ag(111)). These XRD patterns show only the peaks corresponding to metallic silver. The grain sizes of the obtained Ag NPs changes from 22.7 to 30.0 nm when the particle sizes become larger (the amount of PVP becomes smaller). However the difference in grainsize was smaller than the difference in particle size.[35]

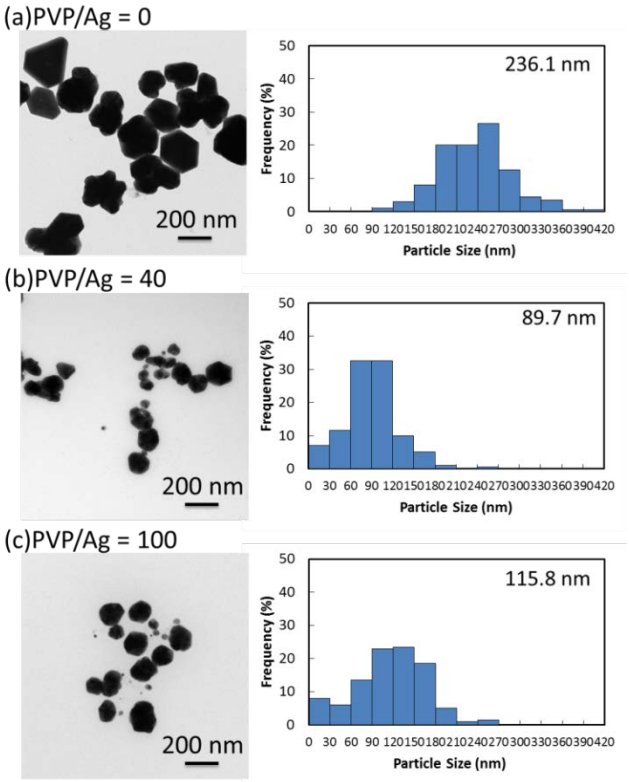

Figure 1 Transmission electron microscopy images and particle size distributions of Ag nanoparticles. The molar ratio of poly(vinyl pyrrolidone) to Ag in the reaction solutions were (a) 0: Sample 1, (b) 40: Sample 2, and (c) 100: Sample 3.

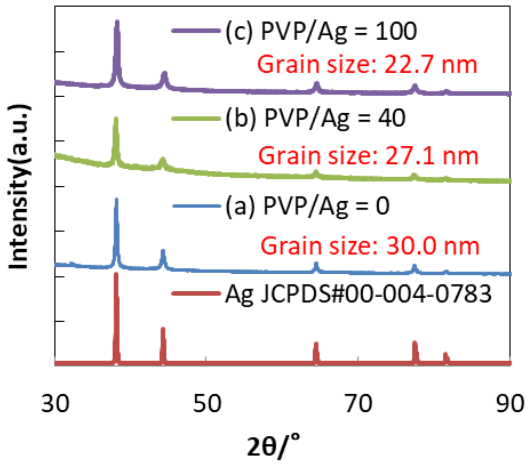

Figure 2 X-ray diffraction patterns of Ag nanoparticles. Grain sizes calculated using Sherrer's equation applied to the largest peak at 38.2° (Ag(111)) was also shown in the pattern. The molar ratio of poly(vinyl pyrrolidone) to Ag in the reaction solutions were (a) 0: Sample 1, (b) 40: Sample 2, and (c) 100: Sample 3. Comparison with the pattern of Ag metal (red) shows that the nanoparticles obtained consisted of metallic Ag.

The proposed nucleation and growth mechanism of the Ag NPs are based on La Mer's model.[36] **Figure 3** shows a schematic illustration of the nucleation and growth mechanism under various PVP concentrations. Nucleation occurs only when the concentration of Ag monomers exceeds the critical supersaturation level. When the concentration of monomers falls below the critical supersaturation level, only particle growth occurs. We considered the effects of aggregation inhibition of small nanoparticles by PVP, and the control of monomer concentration by the reduction rate on the size of the obtained Ag NPs.

Without PVP (PVP/Ag = 0), the surface of the nanoparticles was not covered by a capping agent. Therefore, nanoparticles aggregated, and uncontrolled particle growth occurred (**Figure 3(a)**). As a result, irregular particles of a relatively large size were obtained. When PVP concentration was adjusted to an optimal value (PVP/Ag = 40), spherical and a small amount of polygonal nanoparticles were obtained. The aggregation of small nanoparticles was inhibited by the adsorption of PVP on the nanoparticle surface (**Figure 3(b)**). In many cases of Ag NPs preparation by chemical reduction, polygonal faceted structures can be observed.[37,38] When the PVP concentration was increased (PVP/Ag = 100), a mixture of large spherical particles and small nanoparticles, whose particle size was around 20 nm, was obtained. The diameter of these small nanoparticles is corresponding to the grain size. The reduction rate of $[Ag^+]$ was decreased and the particle growth was inhibited because PVP was strongly adsorbed on the nanoparticle surface (**Figure 3(c)**). As a result, a second nucleation period occurred, and small nanoparticles were generated.

The variation of the grain sizes of the obtained Ag NPs was much smaller than that of the particle sizes. This situation can also be explained also by La Mer's model shown in Fig. 3. In all cases, nucleation stage is almost similar and this stage controls the grain formation. Moreover, the reaction temperature is as low as 80 °C in all cases, the grain formation is almost same in all cases.

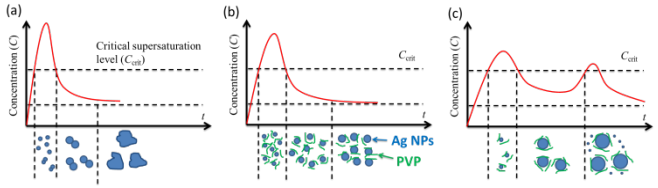

Figure 3 Schematic illustrations of the nucleation and growth mechanisms when the molar ratios of poly(vinyl pyrrolidone) to Ag in the reaction solutions were (a) 0: Sample 1, (b) 40: Sample 2, and (c) 100: Sample 3.

It has been shown that using H_2O_2 as a reductant in Ag particle synthesis can yield fine particles of sizes greater than 1 μm,[21-24] or, in our study, particles on the nanometer scale. In order to form nanoparticles, the $[Ag^+]$ concentration of the reaction solution was lower (0.3 mM). Because $[Ag^+]$ concentration was decreased, aggregation was suppressed and the particle size was decreased.

Effect of Reaction Temperature

Figure 4 shows TEM images and particle size distributions of Ag NPs obtained under various reaction temperatures. When the reaction temperature was adjusted to 50, 80, or 90 °C (Samples 4, 2, and 5, respectively), the average particle sizes were 113.6, 89.7, and 20.8 nm, respectively. X-ray diffraction patterns and grain sizes of the Ag NPs are shown in **Figure 5**. These patterns contain peaks from metallic silver only. Similar to the previous section, the grain sizes of the obtained Ag NPs changes from 26.2 to 31.1 nm when the particle sizes become larger.

The average particle size decreased at higher reaction temperatures. When the reaction temperature was high, the reduction rate was also high. This phenomenon suggests that vigorous nucleation occurred at higher temperatures, and average particle size decreased. When the reaction temperature was kept at 50 °C, both facetted plates and spheres were obtained. This is due to the preferential adsorption of PVP to a specific crystal plane, which inhibited crystal growth. On the other hand, when the reaction temperature was kept at 90 °C, a mixture of spherical particles and very small nanoparticles, whose particle size was around 10 nm, was obtained. Considering the grain size of this sample, the small nanoparticles should be single crystals. At higher temperature reduction of Ag^+ becomes faster at higher temperature. Therefore, formation of nuclei and small Ag NPs capped by PVP is faster at higher temperatures. Therefore, the number of small Ag NPs becomes larger. The speed of particle growth of the Ag NPs capped by PVP would be slow compared to the reduction speed at high temperature.

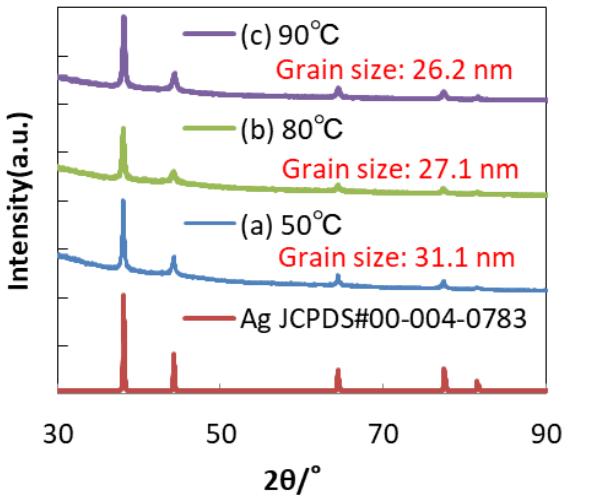

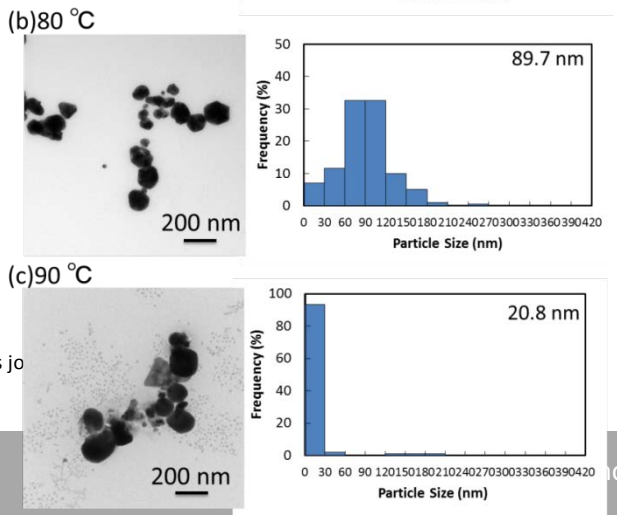

Figure 4 Transmission electron microscopy images and particle size distributions of Ag nanoparticles. The reaction temperature of the reaction solutions were (a) 50 °C: Sample 4, (b) 80 °C: Sample 2, and (c) 90 °C: Sample 5.

Figure 5 X-ray diffraction patterns of Ag nanoparticles. The reaction temperature of the reaction solutions were (a) 50 °C: Sample 4, (b) 80 °C: Sample 2, and (c) 90 °C: Sample 5. Grain sizes calculated using Sherrer's equation applied to the largest peak at 38.2° (Ag(111)) was also shown in the pattern Comparison with the pattern of Ag metal (red) shows that the nanoparticles obtained consisted of metallic Ag.

Effect of pH

Figure 6 shows TEM images and particle size distributions of Ag NPs obtained under various pH values of the reaction solutions. In our case, pH was adjusted in the alkaline region in order to keep $\Delta G°$ negative. Therefore, pH values of 10, 11 and 12 were examined. pH values strongly affected to the particle size of Ag NPs. When the pH values of the reaction solutions were adjusted to 10 and 11 (Samples 2 and 6, respectively), the average particle sizes were 89.7 and 545.7 nm, respectively. When the preparation was carried out at pH of 12 (Sample 7), no clear particle image was obtained by TEM.

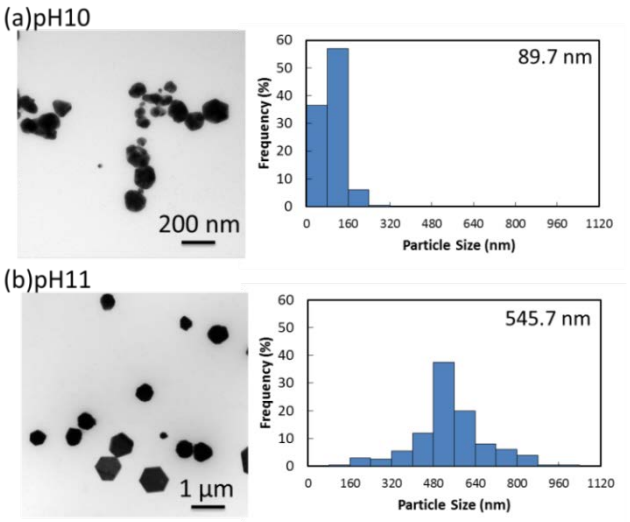

Fig. 6 Transmission electron microscopy images and particle size distributions of Ag nanoparticles. The pH values of the reaction solutions were (a) 10: Sample 2, and (b) 11: Sample 6.

When the pH of the reaction solution was 12 (Sample 7), no obvious colour change was observed even after the reaction. In order to evaluate the reaction rate at pH = 12, we used a AgI-colloid method which was described elsewhere[12] to evaluate the concentration of Ag^+ during the reaction. The calibration curve used for calculating the concentrations of $[Ag^+]$ in the solutions from the absorption peak area of AgI colloid at around 330 nm is shown in **Figure S1**. **Figure S2** shows the UV-Vis spectra after the reduction with and without the addition of KI when the pH of the reaction solution was adjusted to 12. From these spectra, it was calculated that

about 78% of [Ag^+] were not reduced after the reaction. When the pH of the reaction solution was 12, the amount of NH_3 in the reaction solution increased. Therefore, formation of the silver ammine complex became more favorable, and the reduction rate was decreased.

Then, it can be assumed that the large difference of the particle diameter of the Ag NPs obtained at pH of 10 and 11 must be explained the difference of the reduction rate of Ag^+ ions because the pH values were fixed by addition of NH_4OH in the reaction solution. At pH of 11, the reduction rate of Ag^+ should be smaller than that at pH of 10, the number of Ag nuclei considerably decreased at pH of 11. Therefore, the final particle size of Ag NPs obtained at pH of 11 became much larger than that obtained at pH of 10.

X-ray diffraction patterns and grain sizes of the Ag NPs are shown in **Figure 7**. Only peaks from metallic silver were observed in the patterns. When the pH of the reaction solution was 12, XRD could not be measured, because there was not a sufficient amount of Ag NPs for the XRD measurement according to the slow reduction rate. The grain size was not affected much by the pH value of the reaction solution. This phenomenon indicates that the determination factor of the grain size is not the reduction rate of Ag^+.

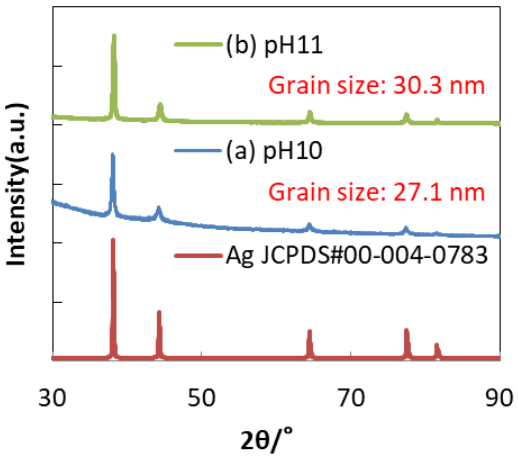

Figure 7 X-ray diffraction patterns of Ag nanoparticles. The pH values of the reaction solutions were (a) 10: Sample 2, and (b) 11: Sample 6. Grain sizes calculated using Sherrer's equation applied to the largest peak at 38.2° (Ag(111)) was also shown in the pattern Comparison with the pattern of Ag metal (red) shows that the nanoparticles obtained consisted of metallic Ag.

Effect of H_2O_2 Concentration

Figure 8 shows TEM images and particle size distributions of Ag NPs obtained under various molar ratios of H_2O_2 to Ag. When the molar ratios of H_2O_2 to Ag was 0.6, 1, or 10 (Samples 8, 9, and 2, respectively), the average particle sizes were 112.5, 125.9, and 89.7 nm, respectively. The H_2O_2 concentration within this range did not drastically affect the reduction rate of the Ag^+ ions. But at H_2O_2/Ag = 10, the particle sizes became smaller. This is probably due to the slightly higher reduction rate of Ag^+ with much excess H_2O_2. Therefore, the particle size of the obtained Ag NPs did not drastically change.

X-ray diffraction patterns and grain sizes obtained using Sherrer's equation of these Ag NPs are collected in **Figure 9**. Only peaks from metallic silver were observed in the patterns even at a very low H_2O_2/Ag ratio of 0.6. (Minimum ratio must be 0.5 as shown in **Eq. 1**) The grain size is not strongly affected by the H_2O_2/Ag ratios because of the small difference of the particle size.

In all preparation conditions, the grain sizes of the obtained Ag NPs are almost similar in the range of 23.3 – 30.0 nm, even the particle sizes widely differ in the range of 20.8 – 545.7 nm. These data strongly suggest that the grain size is mainly controlled by the temperature or the concentration of Ag^+ ions.

Figure 8. Transmission electron microscopy images and particle size distributions of Ag nanoparticles. The molar ratio of H_2O_2 to Ag in the reaction solutions were (a) 0.6: Sample 8, (b) 1: Sample 9, and (c) 10: Sample 2.

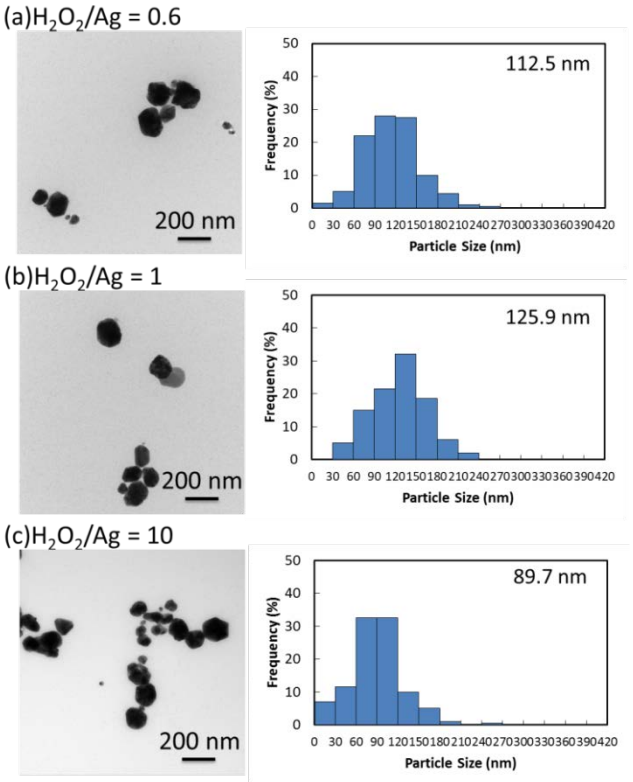

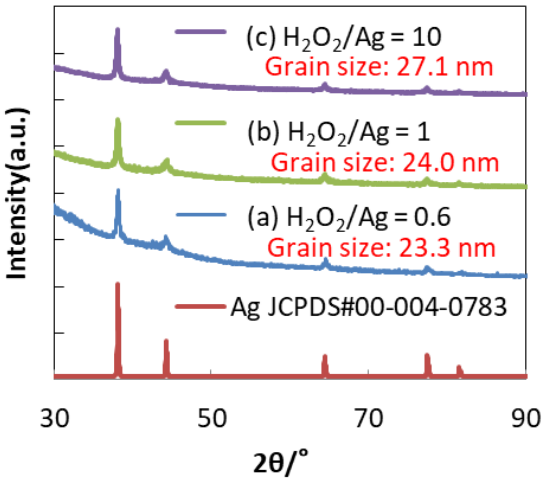

Figure 9. X-ray diffraction patterns and grain sizes of Ag nanoparticles. The molar ratio of H_2O_2 to Ag in the reaction solutions were (a) 0.6: Sample 8, (b) 1: Sample 9, and (c) 10: Sample 2. Grain sizes calculated using Sherrer's equation applied to the largest peak at 38.2° (Ag(111)) was also shown in the pattern Comparison with the pattern of Ag metal (red) shows that the nanoparticles obtained consisted of metallic Ag.

Effect of Silver Precursor

The effect of silver precursors was also investigated. **Figure 10** shows TEM images and particle size distributions of Ag NPs obtained using solid Ag_2O powder as a silver precursor (Sample 10). The PVP/Ag molar ratio, reaction temperature, and pH used 40, 80 °C, and 10, respectively. Homogeneous spherical Ag nanoparticles were obtained. The average particle size was 59.9 nm. The particle size was smaller than those obtained using $AgNO_3$ as the silver precursor. The X-ray diffraction pattern and grain size obtained using Sherrer's equation of Ag NPs are shown in **Figure 11**. The pattern also contains peaks from metallic silver only. The grain size of Ag NPs obtained from Ag_2O as a silver precursor was almost same as that obtained from $AgNO_3$ (Sample 2).

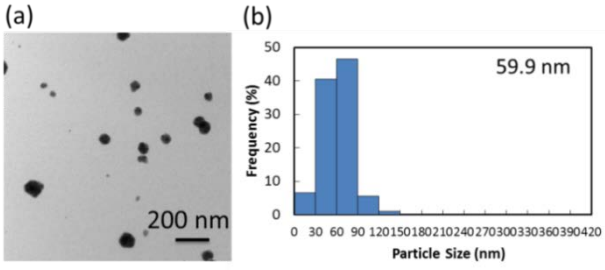

Figure 10 (a) Transmission electron microscopy image, and (b) particle size distribution of Sample 10 Ag nanoparticles prepared using Ag_2O as the silver precursor.

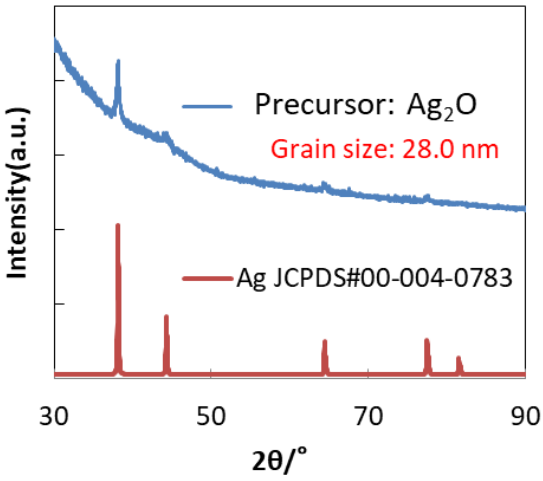

Figure 11 X-ray diffraction pattern and grain size of Sample 10 Ag nanoparticles. The silver precursor was Ag_2O. Grain sizes calculated using Sherrer's equation applied to the largest peak at 38.2° (Ag(111)) was also shown in the pattern Comparison with the pattern of Ag metal (red) shows that the nanoparticles obtained consisted of metallic Ag.

Figure 12 shows a schematic illustration of the progress of the reaction when the silver precursor is Ag_2O. Part of the Ag_2O dissolved as a silver ammine complex before the addition of H_2O_2. However, Ag_2O was also in the reaction solution. After the addition of H_2O_2, the silver ammine complex was reduced rapidly, and free NH_3 molecules were generated. The NH_3 molecules then reacted with Ag_2O to form the silver ammine complex. This reaction was repeated, until the Ag_2O was completely reduced. When using Ag_2O as a silver precursor, the initial $[Ag^+]$ concentration in the solution was lower than when using $AgNO_3$ but it was kept constant during the reduction. The reduction rate of Ag^+ should be smaller than when $AgNO_3$ was used as the precursor. As a result, smaller nanoparticles were obtained when using Ag_2O as a silver precursor. A similar process, the reduction of AgCl by sodiium borohydrate in the presence of thiol compounds was reported elsewhere.[5]

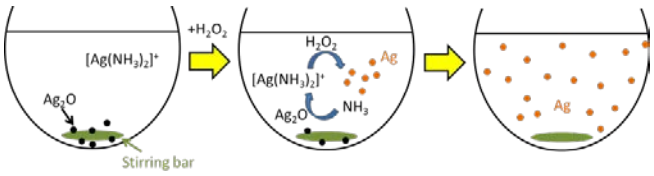

Figure 12 Schematic illustration of the reaction progress when the silver precursor was Ag_2O.

Antibacterial test of Ag NPs

Antibacterial properties were evaluated using Ag NPs prepared at the condition of pH 10 and 11. The particle sizes were about

90 and 500 nm, respectively. **Figure 13 (a)** and **(b)** shows the photographs of the arger plate mediums containing *S. mutans* incubated for 20 hours after the addition of Ag NPs. The particles sizes of Ag NPs were about (A) 90 and (B) 500 nm, respectively. In **Figure 13 (a)**, growth inhibitions were observed around the spot of Ag NPs whose particle size was 90 nm. Small NPs were more effective than big NPs because small NPs have a large surface area. **Figure 13 (b)** indicates that Ag NPs whose particle size was 90 nm show the antibacterial activity with low Ag concentrations.

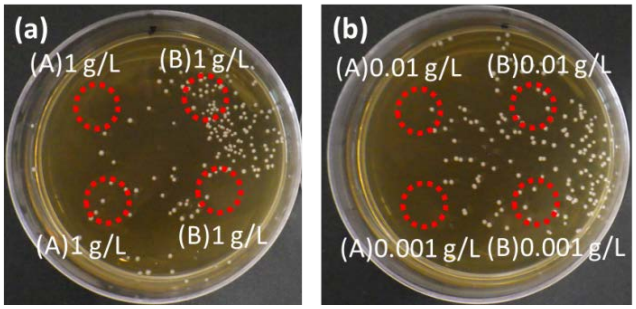

Figure 13 Photographs of the arger plate mediums containing *S. mutans* incubated for 20 hours after the addition of Ag NPs whose particle sizes were about (A) 90 and (B) 500 nm. Red dotted lines show the spot of Ag NPs.

Conclusions

Homogeneous Ag nanoparticles were successfully prepared by a chemical reduction using H_2O_2 as a reducing agent. The PVP concentration, reaction temperature, pH of the reaction solution, and silver precursor had a great influence on the size of the Ag nanoparticles. These parameters affected the reduction rate of the Ag^+ ions, and the aggregation inhibition of the Ag nanoparticles. We tested the antimicrobial properties of Ag NPs against *S. mutans*. The results indicated that the obtained Ag NPs showed the antibacterial activity. These results demonstrate that the formation of Ag nanoparticles does not require the use of toxic reducing agents. Therefore, Ag nanoparticles made using this process will be useful as materials for electronics and plasmonics as well as biomaterials.

Conflicts of interest

There are no conflicts to declare.

Acknowledgements

This work is partially supported by Hokkaido University. Authors thank Dr. Y. Ishida, Dr. M. T. Nguyen, Mr. H. Tsukamoto, Mr. T. Tanioka, and Ms. Y. Yamauchi (Hokkaido University) for fruitful discussions and technical assistance. A part of this work was conducted at Laboratory of XPS analysis, Joint-use facilities, Hokkaido University, and microstructural characterization platforms of Hokkaido University supported by "Nanotechnology Platform" Program of the Ministry of Education, Culture, Sports, Science and Technology (MEXT), Japan.

Notes and references

1 V. K. Sharma, R. A. Yngard and Y. Lin, *Adv. Colloid Interface Sci.*, 2009, **145**, 83-96.
2 L. F. Espinosa-Cristóbal, G. A. Martínez-Castañón, R. E. Martínez-Martínez, J. P. Loyola-Rodríguez, N. Patiño-Marín, J. F. Reyes-Macías, F. Ruiz, *Mater. Lett.*, 2009, **63**, 2603-2606.
3 K. Kawai, T. Narushima, K. Kaneko, H. Kawakami, M. Matsumoto, A. Hyono, H. Nishihara, T. Yonezawa, *Appl. Surf. Sci.*, 2012, **262**, 76-80.
4 W. Shen, X. Zhang, Q. Huang, Q. Xu and W. Song, *Nanoscale*, 2014, **6**, 1622-1628.
5 Y. Li, Y. Wu and B. S. Ong, *J. Am. Chem. Soc.*, 2005, **127**, 3266-3267.
6 A. Kosmala, R. Wright, Q. Zhang and P. Kirby, *Mater. Chem. Phys.*, 2011, **129**, 1075-1080.
7 T. Yonezawa, S. Onoue and N. Kimizuka, *Langmuir*, 2000, **16**, 5218-5220.
8 T. Yonezawa, H. Genda and K. Koumoto, *Chem. Lett.*, 2003, **32**, 194-195.
9 J. S. Kim, E. Kuk, K. N. Yu, J.-H. Kim, S. J. Park, H. J. Lee, S. H. Kim, Y. K. Park, Y. H. Park, C.-Y. Hwang, Y.-K. Kim, Y.-S. Lee, D. H. Jeong and M.-H. Cho, *Nanomed. Nanotechnol. Biol. Med.*, 2007, **3**, 95-101.
10 Y. Hattori, S. Mukasa, H. Toyota, T. Inoue and S. Nomura, *Mater. Chem. Phys.*, 2011, **131**, 425-430.
11 S. Sato, K. Mori, O. Ariyada, H. Atsushi and T. Yonezawa, *Surf. Coat. Technol.*, 2011, **206**, 955-958.
12 M. Nishimoto, H. Tsukamoto, M. T. Nguyen and T. Yonezawa, *ChemistrySelect*, 2017, **2**, 7873-7879.
13 Y. Ishida, R. D. Corpuz and T. Yonezawa, *Acc. Chem. Res.*, 2017, **50**, 2986-2995.
14 Y. Ishida, S. Udagawa and T. Yonezawa, *Colloids Surf. A*, 2016, **498**, 106-111.
15 Y. Ishida, S. Udagawa and T. Yonezawa, *Colloids Surf. A*, 2016, **504**, 437-441.
16 Y. Ishida, R. Nakabayashi, R. D. Corpuz and T. Yonezawa, *Colloids Surf. A*, 2017, **518**, 25-29.
17 A. Pyatenko, K. Shimokawa, M. Yamaguchi, O. Nishimura and M. Suzuki, *Appl. Phys. A*, 2004, **79**, 803-806.
18 T. K. Sarma and A. Chattopadhyay, *Langmuir*, 2004, **20**, 3520-3524.
19 B. R. Panda and A. Chattopadhyay, *J. Nanosci. Nanotechnol.*, 2007, **7**, 1911-1915.
20 X. Liu, H. Xu, H. Xia and D. Wang, *Langmuir*, 2012, **28**, 13720-13726.
21 H. Chen, E. Kern, C. Ziegler and A. Eychmüller, *J. Phys. Chem. C*, 2009, **113**, 19258-19262.
22 H. Gatemala, P. Pienpinijtham, C. Thammacharoen and S. Ekgasit, *CrystEngComm*, 2015, **17**, 5530-5537.
23 H. Gatemala, S. Ekgasit, K. Wongravee, *Chemosphere*, 2017, **178**, 249-258.
24 X. H. Bai, P. Zhang and Z. LIN, *DEStech Transactions on Engineering and Technology Research amita*, 2016.
25 T. Parnklang, C. Lertvachirapaiboon, P. Pienpinijtham, K. Wongravee, C. Thammacharoen and S. Ekgasit, *RSC Adv.*, 2013, **3**, 12886-12894.

26 T. Parnklang, B. Lamlua, H. Gatemala, C. Thammacharoen, S. Kuimalee, B. Lohwongwatana and S. Ekgasit, *Mater. Chem. Phys.*, 2015, **153**, 127-134.
27 Q. Chen, J. Li and Y. Li, *J. Phys. D: Appl. Phys.*, 2015, **48**, 424005.
28 M. Nishimoto, T. Yonezawa, D. Čempel, M. T. Nguyen, Y. Ishida and H. Tsukamoto, *Mater. Chem. Phys.*, 2017, **193**, 7-12.
29 D. Čempel, M. T. Nguyen, Y. Ishida, H. Tsukamoto, H. Shirai, Y. Wang, K. C.-W. Wu and T. Yonezawa, *J. Nanosci. Nanotechnol.*, 2016, **16**, 9257-9262.
30 H. Liu, B. Zhang, H. Shi, Y. Tang, K. Jiao and X. Fu, *J. Mater. Chem.*, 2008, **18**, 2573-2580.
31 N. Toshima and T. Yonezawa, *New J. Chem.*, 1988, **22**, 1179-1201.
32 H. Shirai, M. T. Nguyen, Y. Ishida and T. Yonezawa, *J. Mater. Chem. C*, 2016, **4**, 2228-2234.
33 H. Thiele and H. S. von Levern, *J. Colloid Sci.*, 1965, **20**, 679-694.
34 B. Wiley, Y. Sun, B. Mayers and Y. Xia, *Chem. Eur. J.,* 2005, **11**, 454-463.
35 R. Ma, C. Levard, S. M. Marinakos, Y. Cheng, J. Liu, F. M. Michel, G. E. Brown and G. V. Lowry, *Environ. Sci. Technol.*, 2012, **46**, 752–759.
36 B. K. Park, S. Jeong, D. Kim, J. Moon, S. Lim and J. S. Kim, *J. Colloid Interface Sci.*, 2007, **311**, 417-424.
37 X. Dong, X. Ji, H. Wu, L. Zhao, J. Li and W. Yang, *J. Phys. Chem. C*, 2009, **113**, 6573-6576.
38 I. Pastoriza-Santos and L. M. Liz-Marzán, *Nano Lett.*, 2002, **2**, 903-905.